Editors' Suggestion

Tangent Space Approach for Thermal Tensor Network Simulations of the 2D Hubbard Model

Qiaoyi Li,[1,2,3] Yuan Gao,[1,2] Yuan-Yao He,[4,5,3] Yang Qi,[6,7,3,*] Bin-Bin Chen,[8,†] and Wei Li[2,3,9,10,‡]

[1]School of Physics, Beihang University, Beijing 100191, China
[2]CAS Key Laboratory of Theoretical Physics, Institute of Theoretical Physics, Chinese Academy of Sciences, Beijing 100190, China
[3]Hefei National Laboratory, University of Science and Technology of China, Hefei 230088, China
[4]Institute of Modern Physics, Northwest University, Xi'an 710127, China
[5]Shaanxi Key Laboratory for Theoretical Physics Frontiers, Xi'an 710127, China
[6]State Key Laboratory of Surface Physics and Department of Physics, Fudan University, Shanghai 200433, China
[7]Collaborative Innovation Center of Advanced Microstructures, Nanjing 210093, China
[8]Department of Physics and HKU-UCAS Joint Institute of Theoretical and Computational Physics, The University of Hong Kong, Pokfulam Road, Hong Kong, China
[9]Peng Huanwu Collaborative Center for Research and Education, Beihang University, Beijing 100191, China
[10]CAS Center for Excellence in Topological Quantum Computation, University of Chinese Academy of Sciences, Beijng 100190, China

(Received 11 January 2023; revised 17 March 2023; accepted 25 April 2023; published 1 June 2023)

Accurate simulations of the two-dimensional (2D) Hubbard model constitute one of the most challenging problems in condensed matter and quantum physics. Here we develop a tangent space tensor renormalization group (tanTRG) approach for the calculations of the 2D Hubbard model at finite temperature. An optimal evolution of the density operator is achieved in tanTRG with a mild $O(D^3)$ complexity, where the bond dimension D controls the accuracy. With the tanTRG approach we boost the low-temperature calculations of large-scale 2D Hubbard systems on up to a width-8 cylinder and 10×10 square lattice. For the half-filled Hubbard model, the obtained results are in excellent agreement with those of determinant quantum Monte Carlo (DQMC). Moreover, tanTRG can be used to explore the low-temperature, finite-doping regime inaccessible for DQMC. The calculated charge compressibility and Matsubara Green's function are found to reflect the strange metal and pseudogap behaviors, respectively. The superconductive pairing susceptibility is computed down to a low temperature of approximately $1/24$ of the hopping energy, where we find d-wave pairing responses are most significant near the optimal doping. Equipped with the tangent-space technique, tanTRG constitutes a well-controlled, highly efficient and accurate tensor network method for strongly correlated 2D lattice models at finite temperature.

DOI: 10.1103/PhysRevLett.130.226502

Introduction.—The paradigmatic Hubbard model [1,2] is arguably the most intensively studied lattice model for strongly correlated electrons [3,4]. It has been widely believed to capture the quintessence of high-temperature superconductivity [5–9], and recently also realized in optical lattice quantum simulations [10–15]. The intriguing interplay between the spin and charge degrees of freedom in the Hubbard model may give rise to abundant, even a plethora of electron orders in the finite-temperature phase diagram [16–21]. However, large-scale simulations of the 2D Hubbard model with a broad range of doping and down to low temperature yet constitute a widely open and truly challenging problem [4].

Tensor networks (TNs) and their renormalization group methods provide powerful approaches for quantum many-body problems [22–25]. In particular, thermal TNs [26–31] have been conceived and extensively used in the studies of low-dimensional quantum magnets [32–37] and recently also in correlated fermions at finite temperature [17,38–42]. However, the accessible system size and lowest temperature that fermion thermal TN methods can handle are still rather limited. For a comparison, while the $T = 0$ density matrix renormalization group (DMRG) can deal with fermion cylinders of width $W = 6$–8 [43–46], finite-temperature calculations can currently reach a $W = 4$ Hubbard cylinder [17,40]. For cracking electron secrets in the phase diagram of the 2D Hubbard model, like the strange metallicity [16], pseudogap [17], and d-wave superconductivity [46–50], further developments in the algorithm are highly required.

In this Letter, we propose a tangent space tensor renormalization group (tanTRG) approach for highly controlled simulations both at half filling and finite doping. It has the following promising features: (i) A versatile 2D finite-temperature approach with efficient temperature grid design. Through a quasi-1D mapping, it systematically deals with the long-range interactions and evolves 2D systems based on the matrix product operator (MPO) representation of the Hamiltonian, making it advantageous over the Trotter-based approach [26,27,30,51]. In tanTRG we integrate a flow equation and have a very high degree of flexibility in designing temperature grids. A remarkably

larger imaginary-time step can be taken in tanTRG compared to Trotter-based approaches. (ii) Moderate computational complexity. Compared to the exponential tensor renormalization group (XTRG) that can simulate a 2D system down to low temperatures with a relatively high cost of $O(D^4)$ [29,39], tanTRG is with only $O(D^3)$ complexity that allows for a significantly larger bond dimension D in the calculations. These advantages therefore lead to (iii) unprecedented finite-temperature simulations of large-scale systems. As fermion symmetries can be conveniently implemented in tanTRG with the tensor library QSpace [52–54], it further reduces the computational costs and allows for up to $D^* = 4,096$ $\mathrm{SU}(2)_{\mathrm{charge}} \times \mathrm{SU}(2)_{\mathrm{spin}}$ multiplets at half filling (i.e., approximately $D \approx 25000$ equivalent $\mathrm{U}(1)_{\mathrm{charge}} \times \mathrm{U}(1)_{\mathrm{spin}}$ states). For doped cases, $\mathrm{U}(1)_{\mathrm{charge}} \times \mathrm{SU}(2)_{\mathrm{spin}}$ can also be implemented. Note the spin and charge symmetries can be implemented in the MPO representation of the grand canonical ensemble (GCE) density operator. It helps further enhance the effective bond dimension D and renders excellent accuracy for large-scale Hubbard systems on up to a width-8 cylinder and 10×10 square lattice down to sufficiently low temperature.

Tangent space tensor renormalization group.—Finite-temperature properties are determined by the (unnormalized) density operator $\rho = e^{-\beta H}$ as illustrated in Fig. 1(a), with β the inverse temperature. The imaginary-time evolution equation reads $d\rho/d\beta = -H\rho$, with $-H\rho$ the tangent vector in $T_\rho\mathcal{H}$ (i.e., the tangent space of the full Hilbert space $\mathcal{H}$), which, in general, sticks out of the tangent space $T_\rho\mathcal{M}$ of the MPO manifold $\mathcal{M}$ [see Fig. 1(b)], i.e., the MPO representation of ρ will increase its bond dimension D in the course of induced flow. In conventional thermal TN methods [26,29–31,51], the so-called truncation process is introduced to bring the evolved MPO back to manifold $\mathcal{M}$ with a fixed D.

Alternatively, here we propose to optimize ρ within the MPO manifold $\mathcal{M}$ using the technique of the time-dependent variational principle (TDVP) [60–64], which was originally conceived for real-time evolutions of pure quantum states. For a generalization to density operator ρ, we find the optimal tangent vector X_ρ on the tangent space $T_\rho\mathcal{M}$, i.e.,

$$\frac{d\rho}{d\beta} = \arg\min_{X_\rho \in T_\rho\mathcal{M}} \|X_\rho + H\rho\|, \tag{1}$$

which defines a tangent vector field $\rho \mapsto X_\rho$ that induces the flow of $\rho(\beta)$ exactly on the manifold $\mathcal{M}$. With the MPO parameterization of ρ, the imaginary-time flow equation can be expressed with local tensors (c.f., Supplemental Material (SM) [55])

$$\frac{dA_i}{d\beta} = -H_i^{(1)}A_i + A_i^L H_i^{(0)} S_i, \tag{2}$$

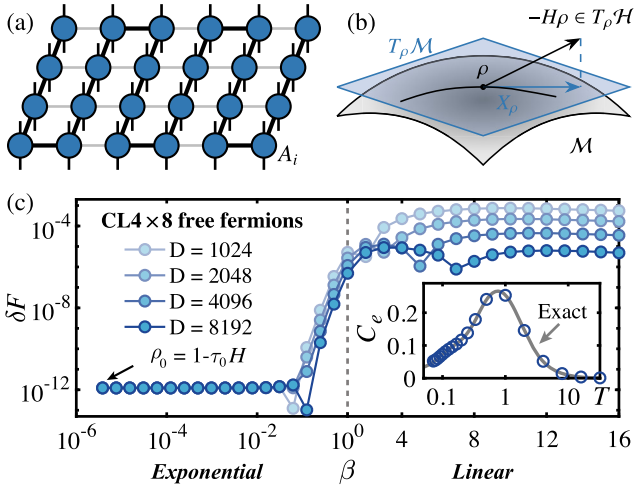

FIG. 1. (a) The MPO representation of thermal density operator ρ and corresponding quasi-1D mapping of the square lattice. The MPO consists of rank-4 tensors A_i with two geometric and two physical indices. (b) The MPO manifold $\mathcal{M}$ and its tangent space $T_\rho\mathcal{M}$, where the black arrow denotes the tangent vector $-H\rho$ for imaginary-time evolution, and the blue one is its component within the tangent space $T_\rho\mathcal{M}$. The flow induced by the projected tangent vector field is indicated by the trajectory within the manifold $\mathcal{M}$. (c) The relative error $\delta F = |F - F_{\mathrm{ex}}|/|F_{\mathrm{ex}}|$ (with F_{ex} the exact solution) for half-filled free fermions on a 4×8 cylinder. A high accuracy is obtained by a hybrid cooling scheme with both exponential ($\beta \leq 1$) and linear ($\beta > 1$) temperature grids. There are two dips in δF that represent cancellation points between different types of errors (see analysis in SM [55]), and the inset shows the specific heat C_e in excellent agreement with the exact solution.

where $H_i^{(1)}$ is the one-site effective Hamiltonian acting on the on-site tensor A_i, and $H_i^{(0)}$ is the bond effective Hamiltonian acting on the bond tensor S_i.

Following the splitting method [65], we separate Eq. (2) into two linear equations $dA_i/d\beta = -H_i^{(1)}A_i$ and $dS_i/d\beta = H_i^{(0)}S_i$ regarding the site and bond updates, respectively, and then integrate the equations sequentially in a sitewise sweep to conduct the time evolution. Taking a left-to-right sweep as an example, we first update the local tensor $A_i(\beta_0 + \tau) = e^{-\tau H_i^{(1)}} A_i(\beta_0)$ with the Lanczos-based exponential method, then left-canonicalize A_i via a QR decomposition $A_i = A_i^L S_i$. Subsequently, we conduct backward evolution of bond tensor $S_i(\beta_0 + \tau) = e^{\tau H_i^{(0)}} S_i(\beta_0)$, associate it to A_{i+1}, and then move on to the next site. Such a sweep process naturally maintains the canonical form of the MPO [55], and guarantees an optimal approximation within its manifold $\mathcal{M}$.

2D Hubbard model on the square lattice.—We consider the single-band Hubbard model on a square lattice, whose Hamiltonian reads

$$H = -t\sum_{\langle i,j\rangle,\sigma}(c_{i\sigma}^\dagger c_{j\sigma} + \mathrm{H.c.}) + U\sum_i n_{i\uparrow}n_{i\downarrow} - \mu\sum_i n_i, \tag{3}$$

where $t = 1$ is chosen as the energy scale, and μ controls the fermion filling n (or hole doping $\delta = 1 - n$). The on-site repulsion is fixed as $U = 8$ if not otherwise mentioned. The calculations are performed on the cylinder lattice (CL) wrapped around the circumference direction (width W) while left open along the longitudinal direction (length L), and also open square (OS) lattice with full open boundaries.

Benchmarks on noninteracting fermions.—We start with benchmarks on free fermions with $U = 0$. The tanTRG calculations can be initialized from a high-temperature density operator $\rho_0 = 1 - \tau_0 H$ with very small $\tau_0 \sim 10^{-6}$, where a compact representation of ρ_0 can be conveniently constructed from the MPO representation of the Hamiltonian [66–70]. After that, we cool down the system by integrating the flow equation, Eq. (2), following flexible temperature grids, and compute the finite-temperature properties from $\rho(\beta)$.

In practice, we always start with exponential grids and exploit the two-site update allowing the MPO bond dimension D to increase adaptively. Successively, a pretty large and constant step length $4\tau = 1$ is adopted in the linear evolution stage. Very accurate results in free energy and specific heat are obtained in Fig. 1(c), as not only the projection but also Lie-Trotter errors are well controlled by bond dimension D [55]. Remember that the free fermion system, though being exactly soluble, poses challenges for TN methods due to the high entanglement associated with the Fermi surface (FS). Here the accurate results on free fermions show that tanTRG provides a powerful tool for tackling more realistic problems.

2D Hubbard model at half filling.—In Fig. 2, we present the tanTRG results on a width-8 cylinder CL8 × 16, and leave the results on narrower cylinders ($W = 4$, 6) to the SM [55]. In practical calculations, we expand ρ_0 to higher orders [69] with a slightly larger $\tau_0 \sim 10^{-4}$, and a bilayer technique is used to compute thermodynamic quantities [71]. In Fig. 2(a) the results of the energy per site ε are found in excellent agreement with the determinant quantum Monte Carlo (DQMC) [72–75] data down to low temperature $T/t \simeq 1/16$ [55].

With the extrapolated ε data, in Fig. 2(b) we show the computed specific heat $C_e = -\beta\partial\varepsilon/\partial \ln \beta$ again fully agrees with the DQMC results. In particular, the two peaks in C_e, i.e., T_h and T_l, respectively, for charge and spin peaks [76–78], constitute two-temperature scales. From the comparisons of CL6 and CL8 data, we find the higher charge peak $T_h/t \sim 2$ has fully converged to the thermodynamic limit and the lower spin peak $T_l/t \sim 0.2$ still changes slightly vs system widths.

As shown in Fig. 2(c), the double occupancy $D_n = (1/N)\sum_i \langle n_{i\uparrow} n_{i\downarrow}\rangle$ (with $N = L \times W$ the total site number) undergoes a rapid decrease at around T_h, indicating the onset of Mott physics. Upon further cooling, the spin-spin correlation $F(d) = (1/N_d)\sum_{\langle i,j\rangle_d} \langle S_i \cdot S_j\rangle$ (i.e., averaged over N_d pairs of sites separated by distance $|i - j| \equiv d$) rises up

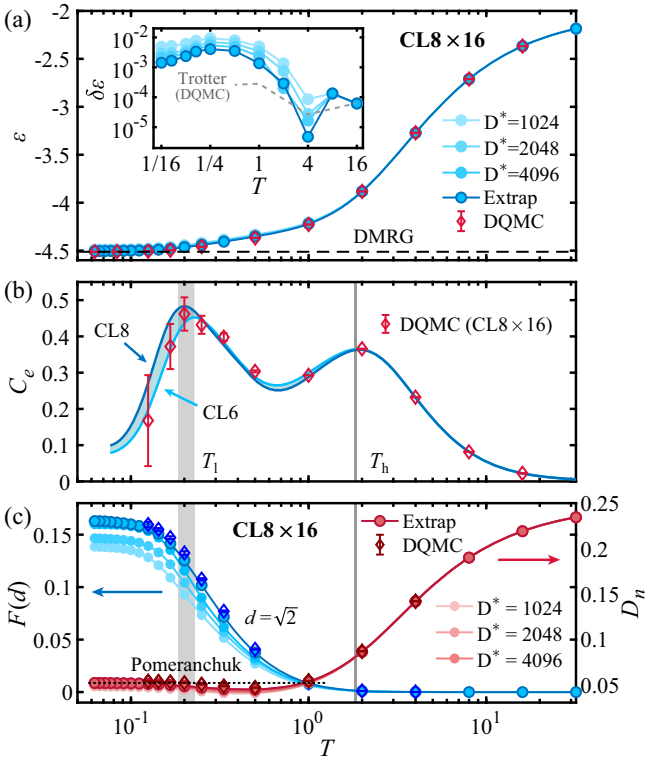

FIG. 2. (a) The results of the half-filled Hubbard model. The relative difference $\delta\varepsilon = |\varepsilon - \varepsilon_{\rm QMC}|/|\varepsilon_{\rm QMC}|$ of the tanTRG results (up to $D^* = 4096$ and extrapolated to infinite D) are plotted vs T in the inset, with the estimated Trotter errors of DQMC also indicated. The ground-state energy is obtained by standard two-site DMRG with $D^* = 8192$ (truncation error $\lesssim 10^{-5}$). (b) The electron specific heat C_e of CL6 × 12 and CL8 × 16, where the two C_e peaks indicate two temperature scales, namely, T_h and T_l. (c) The double occupancy D_n and spin-spin correlations $F(d)$ with $d \equiv \sqrt{2}$, which change rapidly near T_h and T_l, respectively. The anomalous decrease in D_n near T_l as T rises reflects the Pomeranchuk effect in the Hubbard model.

and becomes prominent below T_l. Meanwhile, the double occupancy is found to exhibit a minimum at intermediate temperature $T_l \lesssim T \lesssim T_h$ [78,79]. This can be understood via the Maxwell's relation $(\partial D_n/\partial T)_U = -(\partial S/\partial U)_T$, which associates the anomalous decrease in double occupancy as raising T with the increase of magnetic entropy upon localization by enhancing U. This constitutes an intriguing quantum phenomenon in the Mott phase of Hubbard model [80,81] that resembles the renowned Pomeranchuk effect in ^{3}He.

Charge compressibility at finite doping.—Now we move on to the cases with finite doping. As GCE is adopted in tanTRG simulations, the hole doping δ varies with T and μ (for $\mu \neq U/2$) are shown in Fig. 3(a), again benchmarked with DQMC. For μ slightly lower than $U/2$, e.g., $\mu = 3$, δ approaches zero in the low temperature limit and the sign problem is not very critical for DQMC. In contrast, when μ further deviates $U/2$ and the doping level increases, the

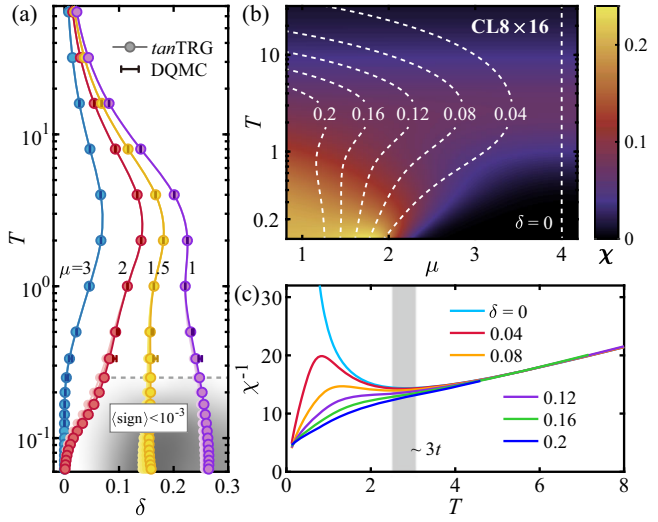

FIG. 3. (a) The doping δ for various T and μ. DQMC is accurate for the lightly doped case or at relatively higher temperature ($T/t > 0.3$) while it is hindered in the shaded regime with $\langle \text{sign} \rangle < 10^{-3}$. tanTRG offers accurate results even below $T/t \simeq 0.06$, under a wide range of dopings. The extrapolation is based on the $D^* = 1024$, 2048, and 2896 data (and up to $D^* = 4096$ for $\mu = 1.5$ case), shown as translucent symbols. (b) The contour plot of compressibility χ, with the equal-δ (dashed) lines also indicated, and (c) plots the inverse compressibility χ^{-1} for various (interpolated) dopings δ.

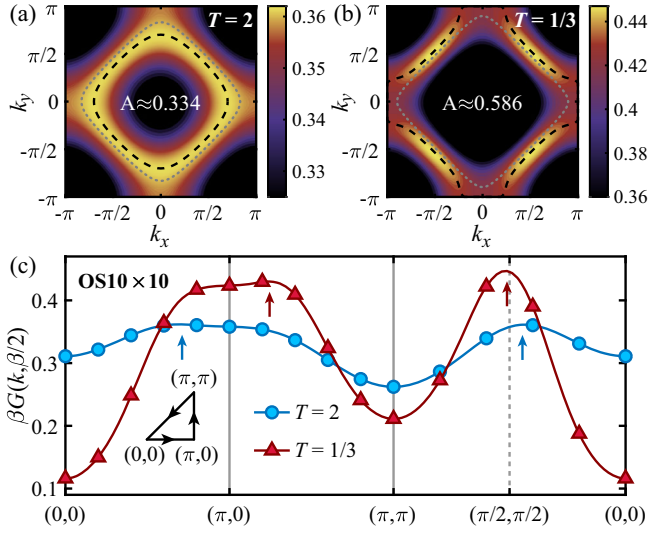

FIG. 4. Topography analysis of $\beta G(k, \beta/2)$ on OS 10×10 lattice with $\mu = 2$ for (a) $T = 2$ (with $\delta \simeq 0.14$) and (b) $T = 1/3$ ($\delta \simeq 0.064$), where the high-quality data are obtained with $D^* = 4096$. The dashed lines connect the maximum of $\beta G(k, \beta/2)$ and indicate the FS, whose enclosed area is denoted as A [with area of the first Brillouin zone (BZ) as unit 1]. The dotted line represents the FS in the noninteracting limit and with the same doping. (c) The triangular path in the BZ: At $T = 2$ the two maxima are located in the interval $[(0,0),(\pi,0)]$ and $[(\pi/2,\pi/2),(0,0)]$, indicating an electronlike FS; while for $T = 1/3$, the two maxima move respectively to the interval $[(\pi,0),(\pi,\pi)]$ and $[(\pi,\pi),(\pi/2,\pi/2)]$ for a holelike FS.

DQMC sign problem becomes severe (i.e., $\langle \text{sign} \rangle < 10^{-3}$, c.f., Supplemental Material Fig. S14 [55]).

As shown in Fig. 3(a), tanTRG produces accordant data in the regime where DQMC works well, and can "penetrate" into the shaded low-T regime inaccessible for DQMC. From Fig. 3(a) we note the electron density is most strongly fluctuating near $\delta \sim 0.1$–0.2, as evidenced by the large compressibility $\chi = (\partial n/\partial \mu)_T$ appearing at intermediate doping and low T in Figs. 3(b) and 3(c). We plot the inverse compressibility χ^{-1} in Fig. 3(c) for various dopings, where the χ^{-1} results exhibit universal linear-T behaviors for $T/t \gtrsim 3$ with little doping dependence. Considering that the compressibility χ has an intimate relation to dc resistivity via the Nernst-Einstein relation, the universal behaviors of χ^{-1} account for the linearity of resistivity in the high-temperature ($T/t \gtrsim 3$) regime. Below $T/t \sim 3$, distinct χ^{-1} behaviors of the Mott insulator and bad metals can be clearly observed. In particular, χ^{-1} is found to converge to a nonzero constant for $T/t \sim 0.1$, which is argued to be related to the second, doping-dependent linear-T regime of resistivity controlled instead by the diffusivity [16].

Matsubara Green's function and Fermi surface topology.—Below the crossover temperature scale $T/t \sim 3$, the inverse compressibility χ^{-1} exhibits a maximum in Figs. 3(b) and 3(c) for the slightly doped case, e.g., $\delta = 0.04$, 0.08, which suggests a dramatic change in the FS upon cooling. For this we compute the single-particle Matsubara Green's function $G(k, \beta/2) = \sum_\sigma \langle e^{\beta H/2} c^\dagger_{k\sigma} e^{-\beta H/2} c_{k\sigma} \rangle_\beta$ with $c_{k\sigma} = (1/\sqrt{N}) \sum_r e^{-ikr} c_{r\sigma}$ [82] that reflects the spectral weight near the FS through $\beta G(k, \beta/2) \sim A(k, \omega = 0)$ at low temperature [83,84]. In Fig. 4, we show the results of $\beta G(k, \beta/2)$ in a slightly doped case, and find quite peculiar temperature evolution of the FS. Despite some blurring due to thermal fluctuations, an electronlike FS with enclosed area $A < 1/2$ can be observed. As the temperature ramps down, an "interacting Lifshitz transition" [18,85,86] occurs. A holelike FS with enclosed area $A > 1/2$ appears in Fig. 4(b), with the boundary "pushed" outwards with respect to the free-fermion FS. The unexpected holelike FS seems to violate the Luttinger theorem and echoes the conclusion in Refs. [19,20,87,88]—the FS topology change can be associated with the opening of a pseudogap. Moreover, we find the signature of the pseudogap gets clearer when the system size increases, and it becomes very prominent when a next nearest hopping t' is introduced [55].

d-wave pairing response.—Next we compute the superconductive pairing responses by applying a pairing field $-h_p \Delta_{\text{tot}} \equiv -h_p \sum_{\langle i,j \rangle} s_{ij} (\Delta_{ij} + \Delta^\dagger_{ij})/2$, where $\Delta_{ij} = (c_{i\downarrow} c_{j\uparrow} - c_{i\uparrow} c_{j\downarrow})/\sqrt{2}$, and $s_{ij} = 1(-1)$ for horizontal (vertical) bonds (c.f., inset in Fig. 5). The results of pairing

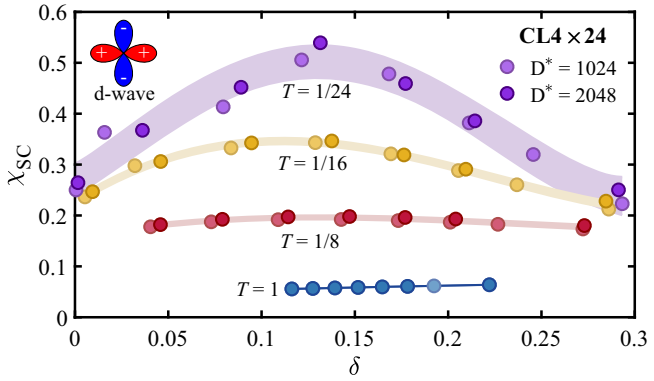

FIG. 5. Pairing susceptibility of the CL4 × 24 Hubbard model with various dopings and temperatures. A pairing field $h_p = 0.01$ is adopted in the calculations, with non-Abelian $Z_{2,\mathrm{charge}} \times \mathrm{SU}(2)_{\mathrm{spin}}$ symmetry implemented. The computed χ_{SC} vs δ fall into the background stripes estimated from the polynomial fittings, whose widths represent the ($\pm\sigma$) confidence intervals.

susceptibility $\langle\Delta_{\mathrm{tot}}\rangle_T/(N_p h_p)$ (with N_p the bond number) are shown in Fig. 5. At relatively high temperature, e.g., $T/t = 1$ and $1/8$, χ_{SC} values are small and insensitive to dopings. However, as the temperature further decreases to $T/t \lesssim 1/16$, χ_{SC} displays a domelike shape with prominent responses near optimal doping $\delta_x \approx 1/8$. Moreover, the induced superconductive order parameter $\langle\Delta_{\mathrm{tot}}\rangle_T/N_p$ is found to vanish as $h_p \to 0$, even for the lowest accessed temperature. Instead, charge stripes and spin correlation modulations appear for $T \lesssim 1/32$ [55]. These results, in full agreement with previous studies [21,45,89,90], show that the ground-state features can be well captured by tanTRG calculations down to sufficiently low temperature.

Summary and outlook.—With tangent-space techniques, we evolve the density operator ρ optimally on the MPO manifold and propose a powerful approach for exploring 2D many-electron problems. We study the intriguing behaviors of charge compressibility that reflect strange metallicity, and unveil a holelike FS in the pseudogap regime. The d-wave pairing responses are computed down to $T/t = 1/24$, which are otherwise rather challenging to obtain for the 2D Hubbard model.

This approach has a wide variety of features. It can reach a low-temperature doped regime that is inaccessible for DQMC, and the $O(D^3)$ complexity, together with the implementation of non-Abelian symmetries, enables tanTRG to deal with wide $W = 8$ cylinders at finite temperature. This is clearly beyond the current limit of $W = 4$ [17,40], where tanTRG obtains results in agreement with minimally entangled typical thermal states (METTS) [17,27,28] (see comparisons in SM [55]). Overall, our results close the gap between thermal TN and ground-state DMRG calculations in terms of system size. As the cylinder width $W > 4$ is important for observing 2D correlation physics [45–50,91], we believe tanTRG will play an active role in exploring the intriguing temperature-doping phase diagrams, and help establish solid connections between theories of high-T_c superconductivity with fundamental models of correlated electrons.

The authors are indebted to Dai-Wei Qu, Shou-Shu Gong, Lei Wang, Wei Wu, Zi Yang Meng, and Tao Shi for helpful discussions. This work was supported by the National Natural Science Foundation of China (Grants No. 12222412, No. 11974036, No. 11834014, No. 12047503, No. 12204377, and No. 12174068), CAS Project for Young Scientists in Basic Research (Grant No. YSBR-057), and the Innovation Program for Quantum Science and Technology (under Grant No. 2021ZD0301900). We thank HPC at ITP-CAS and HPC2021 at the University of Hong Kong for the technical support and generous allocation of CPU time.

*qiyang@fudan.edu.cn
†bchenhku@hku.hk
‡w.li@itp.ac.cn

[1] J. Hubbard, Electron correlations in narrow energy bands, Proc. R. Soc. A **276**, 238 (1963).
[2] M. C. Gutzwiller, Effect of Correlation on the Ferromagnetism of Transition Metals, Phys. Rev. Lett. **10**, 159 (1963).
[3] D. P. Arovas, E. Berg, S. A. Kivelson, and S. Raghu, The Hubbard model, Annu. Rev. Condens. Matter Phys. **13**, 239 (2022).
[4] M. Qin, T. Schäfer, S. Andergassen, P. Corboz, and E. Gull, The Hubbard model: A computational perspective, Annu. Rev. Condens. Matter Phys. **13**, 275 (2022).
[5] J. G. Bednorz and K. A. Müller, Possible high T_c superconductivity in the Ba-La-Cu-O system, Z. Phys. B **64**, 189 (1986).
[6] C. C. Tsuei and J. R. Kirtley, Pairing symmetry in cuprate superconductors, Rev. Mod. Phys. **72**, 969 (2000).
[7] P. A. Lee, N. Nagaosa, and X.-G. Wen, Doping a Mott insulator: Physics of high-temperature superconductivity, Rev. Mod. Phys. **78**, 17 (2006).
[8] B. Keimer, S. A. Kivelson, M. R. Norman, S. Uchida, and J. Zaanen, From quantum matter to high-temperature superconductivity in copper oxides, Nature (London) **518**, 179 (2015).
[9] C. Proust and L. Taillefer, The remarkable underlying ground states of cuprate superconductors, Annu. Rev. Condens. Matter Phys. **10**, 409 (2019).
[10] M. F. Parsons, A. Mazurenko, C. S. Chiu, G. Ji, D. Greif, and M. Greiner, Site-resolved measurement of the spin-correlation function in the Fermi-Hubbard model, Science **353**, 1253 (2016).
[11] D. Greif, M. F. Parsons, A. Mazurenko, C. S. Chiu, S. Blatt, F. Huber, G. Ji, and M. Greiner, Site-resolved imaging of a fermionic Mott insulator, Science **351**, 953 (2016).
[12] L. W. Cheuk, M. A. Nichols, K. R. Lawrence, M. Okan, H. Zhang, E. Khatami, N. Trivedi, T. Paiva, M. Rigol, and M. W. Zwierlein, Observation of spatial charge and spin correlations in the 2D Fermi-Hubbard model, Science **353**, 1260 (2016).

[13] A. Mazurenko, C. S. Chiu, G. Ji, M. F. Parsons, M. Kanász-Nagy, R. Schmidt, F. Grusdt, E. Demler, D. Greif, and M. Greiner, A cold-atom Fermi–Hubbard antiferromagnet, Nature (London) **545**, 462 (2017).

[14] J. Koepsell, D. Bourgund, P. Sompet, S. Hirthe, A. Bohrdt, Y. Wang, F. Grusdt, E. Demler, G. Salomon, C. Gross, and I. Bloch, Microscopic evolution of doped Mott insulators from polaronic metal to Fermi liquid, Science **374**, 82 (2021).

[15] P. Sompet, S. Hirthe, D. Bourgund, T. Chalopin, J. Bibo, J. Koepsell, P. Bojović, R. Verresen, F. Pollmann, G. Salomon, C. Gross, T. A. Hilker, and I. Bloch, Realizing the symmetry-protected Haldane phase in Fermi-Hubbard ladders, Nature (London) **606**, 484 (2022).

[16] E. W. Huang, R. Sheppard, B. Moritz, and T. P. Devereaux, Strange metallicity in the doped Hubbard model, Science **366**, 987 (2019).

[17] A. Wietek, Y.-Y. He, S. R. White, A. Georges, and E. M. Stoudenmire, Stripes, Antiferromagnetism, and the Pseudogap in the Doped Hubbard Model at Finite Temperature, Phys. Rev. X **11**, 031007 (2021).

[18] A. N. Rubtsov, M. I. Katsnelson, A. I. Lichtenstein, and A. Georges, Dual fermion approach to the two-dimensional Hubbard model: Antiferromagnetic fluctuations and Fermi arcs, Phys. Rev. B **79**, 045133 (2009).

[19] W. Wu, M. S. Scheurer, S. Chatterjee, S. Sachdev, A. Georges, and M. Ferrero, Pseudogap and Fermi-Surface Topology in the Two-Dimensional Hubbard Model, Phys. Rev. X **8**, 021048 (2018).

[20] M. S. Scheurer, S. Chatterjee, W. Wu, M. Ferrero, A. Georges, and S. Sachdev, Topological order in the pseudogap metal, Proc. Natl. Acad. Sci. U.S.A. **115**, E3665 (2018).

[21] B. Xiao, Y.-Y. He, A. Georges, and S. Zhang, Temperature Dependence of Spin and Charge Orders in the Doped Two-Dimensional Hubbard Model, Phys. Rev. X **13**, 011007 (2023).

[22] S. R. White, Density Matrix Formulation for Quantum Renormalization Groups, Phys. Rev. Lett. **69**, 2863 (1992).

[23] F. Verstraete, J. J. García-Ripoll, and J. I. Cirac, Matrix Product Density Operators: Simulation of Finite-Temperature and Dissipative Systems, Phys. Rev. Lett. **93**, 207204 (2004).

[24] U. Schollwöck, The density-matrix renormalization group in the age of matrix product states, Ann. Phys. (Amsterdam) **326**, 96 (2011).

[25] J. I. Cirac, D. Pérez-García, N. Schuch, and F. Verstraete, Matrix product states and projected entangled pair states: Concepts, symmetries, theorems, Rev. Mod. Phys. **93**, 045003 (2021).

[26] A. E. Feiguin and S. R. White, Finite-temperature density matrix renormalization using an enlarged Hilbert space, Phys. Rev. B **72**, 220401(R) (2005).

[27] S. R. White, Minimally Entangled Typical Quantum States at Finite Temperature, Phys. Rev. Lett. **102**, 190601 (2009).

[28] E. M. Stoudenmire and S. R. White, Minimally entangled typical thermal state algorithms, New J. Phys. **12**, 055026 (2010).

[29] B.-B. Chen, L. Chen, Z. Chen, W. Li, and A. Weichselbaum, Exponential Thermal Tensor Network Approach for Quantum Lattice Models, Phys. Rev. X **8**, 031082 (2018).

[30] W. Li, S.-J. Ran, S.-S. Gong, Y. Zhao, B. Xi, F. Ye, and G. Su, Linearized Tensor Renormalization Group Algorithm for the Calculation of Thermodynamic Properties of Quantum Lattice Models, Phys. Rev. Lett. **106**, 127202 (2011).

[31] P. Czarnik, L. Cincio, and J. Dziarmaga, Projected entangled pair states at finite temperature: Imaginary time evolution with Ancillas, Phys. Rev. B **86**, 245101 (2012).

[32] T. Xiang, Thermodynamics of quantum Heisenberg spin chains, Phys. Rev. B **58**, 9142 (1998).

[33] L. Chen, D.-W. Qu, H. Li, B.-B. Chen, S.-S. Gong, J. von Delft, A. Weichselbaum, and W. Li, Two-temperature scales in the triangular-lattice Heisenberg antiferromagnet, Phys. Rev. B **99**, 140404(R) (2019).

[34] H. Li, Y. D. Liao, B.-B. Chen, X.-T. Zeng, X.-L. Sheng, Y. Qi, Z. Y. Meng, and W. Li, Kosterlitz-Thouless melting of magnetic order in the triangular quantum Ising material $TmMgGaO_4$, Nat. Commun. **11**, 1111 (2020).

[35] H. Li, H.-K. Zhang, J. Wang, H.-Q. Wu, Y. Gao, D.-W. Qu, Z.-X. Liu, S.-S. Gong, and W. Li, Identification of magnetic interactions and high-field quantum spin liquid in α-$RuCl_3$, Nat. Commun. **12**, 4007 (2021).

[36] S. Yu, Y. Gao, B.-B. Chen, and W. Li, Learning the effective spin Hamiltonian of a quantum magnet, Chin. Phys. Lett. **38**, 097502 (2021).

[37] J. L. Jiménez, S. P. G. Crone, E. Fogh, M. E. Zayed, R. Lortz, E. Pomjakushina, K. Conder, A. M. Läuchli, L. Weber, S. Wessel, A. Honecker, B. Normand, C. Rüegg, P. Corboz, H. M. Rønnow, and F. Mila, A quantum magnetic analogue to the critical point of water, Nature (London) **592**, 370 (2021).

[38] P. Czarnik, M. M. Rams, and J. Dziarmaga, Variational tensor network renormalization in imaginary time: Benchmark results in the Hubbard model at finite temperature, Phys. Rev. B **94**, 235142 (2016).

[39] B.-B. Chen, C. Chen, Z. Chen, J. Cui, Y. Zhai, A. Weichselbaum, J. von Delft, Z. Y. Meng, and W. Li, Quantum many-body simulations of the two-dimensional Fermi-Hubbard model in ultracold optical lattices, Phys. Rev. B **103**, L041107 (2021).

[40] A. Wietek, R. Rossi, F. Šimkovic, M. Klett, P. Hansmann, M. Ferrero, E. M. Stoudenmire, T. Schäfer, and A. Georges, Mott Insulating States with Competing Orders in the Triangular Lattice Hubbard Model, Phys. Rev. X **11**, 041013 (2021).

[41] X. Lin, B.-B. Chen, W. Li, Z. Y. Meng, and T. Shi, Exciton Proliferation and Fate of the Topological Mott Insulator in a Twisted Bilayer Graphene Lattice Model, Phys. Rev. Lett. **128**, 157201 (2022).

[42] A. Sinha, M. M. Rams, P. Czarnik, and J. Dziarmaga, Finite-temperature tensor network study of the Hubbard model on an infinite square lattice, Phys. Rev. B **106**, 195105 (2022).

[43] J. P. F. LeBlanc, A. E. Antipov, F. Becca, I. W. Bulik, G. K.-L. Chan *et al.* (Simons Collaboration on the Many-Electron Problem), Solutions of the Two-Dimensional Hubbard Model: Benchmarks and Results from a Wide Range of Numerical Algorithms, Phys. Rev. X **5**, 041041 (2015).

[44] B.-X. Zheng, C.-M. Chung, P. Corboz, G. Ehlers, M.-P. Qin, R. M. Noack, H. Shi, S. R. White, S. Zhang, and

G. K.-L. Chan, Stripe order in the underdoped region of the two-dimensional Hubbard model, Science **358**, 1155 (2017).
[45] M. Qin, C.-M. Chung, H. Shi, E. Vitali, C. Hubig, U. Schollwöck, S. R. White, and S. Zhang (Simons Collaboration on the Many-Electron Problem), Absence of Superconductivity in the Pure Two-Dimensional Hubbard Model, Phys. Rev. X **10**, 031016 (2020).
[46] S. Jiang, D. J. Scalapino, and S. R. White, Ground-state phase diagram of the $t-t'-J$ model, Proc. Natl. Acad. Sci. U.S.A. **118**, e2109978118 (2021).
[47] H. C. Jiang and T. P. Devereaux, Superconductivity in the doped Hubbard model and its interplay with next-nearest hopping t', Science **365**, 1424 (2019).
[48] Y.-F. Jiang, J. Zaanen, T. P. Devereaux, and H.-C. Jiang, Ground state phase diagram of the doped Hubbard model on the four-leg cylinder, Phys. Rev. Res. **2**, 033073 (2020).
[49] H.-C. Jiang and S. A. Kivelson, High Temperature Superconductivity in a Lightly Doped Quantum Spin Liquid, Phys. Rev. Lett. **127**, 097002 (2021).
[50] S. Gong, W. Zhu, and D. N. Sheng, Robust d-wave Superconductivity in the Square-Lattice $t-J$ Model, Phys. Rev. Lett. **127**, 097003 (2021).
[51] M. Zwolak and G. Vidal, Mixed-State Dynamics in One-Dimensional Quantum Lattice Systems: A Time-Dependent Superoperator Renormalization Algorithm, Phys. Rev. Lett. **93**, 207205 (2004).
[52] A. Weichselbaum, Non-Abelian symmetries in tensor networks: A quantum symmetry space approach, Ann. Phys. (Amsterdam) **327**, 2972 (2012).
[53] A. Weichselbaum, X-symbols for non-Abelian symmetries in tensor networks, Phys. Rev. Res. **2**, 023385 (2020).
[54] B. Bruognolo, J.-W. Li, J. von Delft, and A. Weichselbaum, A beginner's guide to non-Abelian iPEPS for correlated fermions, SciPost Phys. Lect. Notes, 25 (2021).
[55] See Supplemental Material at http://link.aps.org/supplemental/10.1103/PhysRevLett.130.226502, Sec. I shows tanTRG results on width-4 and 6 cylinders, Matsubara Green's function, d-wave pairing responses, spin and charge correlations, and the numerical error analysis. Section II describes the MPO flow equation, Lanczos-based exponential method, and the Lie-Trotter splitting. Section III is devoted to details of the DQMC calculations. The Supplemental Material includes Refs. [56–59].
[56] A. J. Dunnett and A. W. Chin, Efficient bond-adaptive approach for finite-temperature open quantum dynamics using the one-site time-dependent variational principle for matrix product states, Phys. Rev. B **104**, 214302 (2021).
[57] J.-W. Li, A. Gleis, and J. von Delft, Time-dependent variational principle with controlled bond expansion for matrix product states, arXiv:2208.10972.
[58] H. F. Trotter, On the product of semi-groups of operators, Proc. Am. Math. Soc. **10**, 545 (1959).
[59] M. Suzuki, Relationship between d-dimensional quantal spin systems and $(d+1)$-dimensional Ising systems—equivalence, critical exponents and systematic approximants of the partition function and spin correlations—, Prog. Theor. Phys. **56**, 1454 (1976).
[60] J. Haegeman, J. I. Cirac, T. J. Osborne, I. Pižorn, H. Verschelde, and F. Verstraete, Time-Dependent Variational Principle for Quantum Lattices, Phys. Rev. Lett. **107**, 070601 (2011).
[61] J. Haegeman, M. Mariën, T. J. Osborne, and F. Verstraete, Geometry of matrix product states: Metric, parallel transport, and curvature, J. Math. Phys. (N.Y.) **55**, 021902 (2014).
[62] J. Haegeman, C. Lubich, I. Oseledets, B. Vandereycken, and F. Verstraete, Unifying time evolution and optimization with matrix product states, Phys. Rev. B **94**, 165116 (2016).
[63] M. Yang and S. R. White, Time-dependent variational principle with ancillary Krylov subspace, Phys. Rev. B **102**, 094315 (2020).
[64] L. Hackl, T. Guaita, T. Shi, J. Haegeman, E. Demler, and J. I. Cirac, Geometry of variational methods: Dynamics of closed quantum systems, SciPost Phys. **9**, 048 (2020).
[65] E. Hairer, G. Wanner, and C. Lubich, *Geometric Numerical Integration*, 2nd ed. (Springer Berlin, Heidelberg, 2006), 10.1007/3-540-30666-8.
[66] F. Fröwis, V. Nebendahl, and W. Dür, Tensor operators: Constructions and applications for long-range interaction systems, Phys. Rev. A **81**, 062337 (2010).
[67] B. Pirvu, V. Murg, J. I. Cirac, and F. Verstraete, Matrix product operator representations, New J. Phys. **12**, 025012 (2010).
[68] C. Hubig, I. P. McCulloch, and U. Schollwöck, Generic construction of efficient matrix product operators, Phys. Rev. B **95**, 035129 (2017).
[69] B.-B. Chen, Y.-J. Liu, Z. Chen, and W. Li, Series-expansion thermal tensor network approach for quantum lattice models, Phys. Rev. B **95**, 161104(R) (2017).
[70] B.-B. Chen, L. Chen, Z. Chen, W. Li, and A. Weichselbaum, Exponential Thermal Tensor Network Approach for Quantum Lattice Models, Phys. Rev. X **8**, 031082 (2018).
[71] Y.-L. Dong, L. Chen, Y.-J. Liu, and W. Li, Bilayer linearized tensor renormalization group approach for thermal tensor networks, Phys. Rev. B **95**, 144428 (2017).
[72] R. Blankenbecler, D. J. Scalapino, and R. L. Sugar, Monte Carlo calculations of coupled boson-fermion systems. I, Phys. Rev. D **24**, 2278 (1981).
[73] J. E. Hirsch, Discrete Hubbard-Stratonovich transformation for fermion lattice models, Phys. Rev. B **28**, 4059 (1983).
[74] J. E. Hirsch, Two-dimensional Hubbard model: Numerical simulation study, Phys. Rev. B **31**, 4403 (1985).
[75] F. Assaad and H. Evertz, World-line and determinantal quantum Monte Carlo methods for spins, phonons and electrons, in *Computational Many-Particle Physics*, edited by H. Fehske, R. Schneider, and A. Weiße (Springer Berlin Heidelberg, Berlin, Heidelberg, 2008), pp. 277–356, 10.1007/978-3-540-74686-7_10.
[76] D. Duffy and A. Moreo, Specific heat of the two-dimensional Hubbard model, Phys. Rev. B **55**, 12918 (1997).
[77] T. Paiva, R. T. Scalettar, C. Huscroft, and A. K. McMahan, Signatures of spin and charge energy scales in the local moment and specific heat of the half-filled two-dimensional Hubbard model, Phys. Rev. B **63**, 125116 (2001).
[78] J. P. F. LeBlanc and E. Gull, Equation of state of the fermionic two-dimensional Hubbard model, Phys. Rev. B **88**, 155108 (2013).

[79] T. Paiva, R. Scalettar, M. Randeria, and N. Trivedi, Fermions in 2D Optical Lattices: Temperature and Entropy Scales for Observing Antiferromagnetism and Superfluidity, Phys. Rev. Lett. **104**, 066406 (2010).

[80] F. Werner, O. Parcollet, A. Georges, and S. R. Hassan, Interaction-Induced Adiabatic Cooling and Antiferromagnetism of Cold Fermions in Optical Lattices, Phys. Rev. Lett. **95**, 056401 (2005).

[81] Z. Cai, H.-h. Hung, L. Wang, D. Zheng, and C. Wu, Pomeranchuk Cooling of SU($2N$) Ultracold Fermions in Optical Lattices, Phys. Rev. Lett. **110**, 220401 (2013).

[82] Note that k is no longer a good quantum number under the open boundary condition, and thus there exist $k' \neq k$ s.t. $G(k, k', \beta/2) \neq 0$. Nevertheless, we find that the off-diagonal components are negligible, i.e., about 1% of total weights at $T = 2$ and 8% at $T = 1/3$.

[83] W. Jiang, Y. Liu, A. Klein, Y. Wang, K. Sun, A. V. Chubukov, and Z. Y. Meng, Monte Carlo study of the pseudogap and superconductivity emerging from quantum magnetic fluctuations, Nat. Commun. **13**, 2655 (2022).

[84] S. Lederer, Y. Schattner, E. Berg, and S. A. Kivelson, Superconductivity and non-Fermi liquid behavior near a nematic quantum critical point, Proc. Natl. Acad. Sci. U.S.A. **114**, 4905 (2017).

[85] K.-S. Chen, Z. Y. Meng, T. Pruschke, J. Moreno, and M. Jarrell, Lifshitz transition in the two-dimensional Hubbard model, Phys. Rev. B **86**, 165136 (2012).

[86] S. Sakai, Y. Motome, and M. Imada, Evolution of Electronic Structure of Doped Mott Insulators: Reconstruction of Poles and Zeros of Green's Function, Phys. Rev. Lett. **102**, 056404 (2009).

[87] V. F. Maisi, S. V. Lotkhov, A. Kemppinen, A. Heimes, J. T. Muhonen, and J. P. Pekola, Excitation of Single Quasiparticles in a Small Superconducting Al Island Connected to Normal-Metal Leads by Tunnel Junctions, Phys. Rev. Lett. **111**, 147001 (2013).

[88] N. Doiron-Leyraud, O. Cyr-Choinière, S. Badoux, A. Ataei, C. Collignon, A. Gourgout, S. Dufour-Beauséjour, F. F. Tafti, F. Laliberté, M. E. Boulanger, M. Matusiak, D. Graf, M. Kim, J. S. Zhou, N. Momono, T. Kurosawa, H. Takagi, and L. Taillefer, Pseudogap phase of cuprate superconductors confined by Fermi surface topology, Nat. Commun. **8**, 2044 (2017).

[89] H.-C. Jiang and S. A. Kivelson, Stripe order enhanced superconductivity in the Hubbard model, Proc. Natl. Acad. Sci. U.S.A. **119**, e2109406119 (2022).

[90] H. Xu, H. Shi, E. Vitali, M. Qin, and S. Zhang, Stripes and spin-density waves in the doped two-dimensional Hubbard model: Ground state phase diagram, Phys. Rev. Res. **4**, 013239 (2022).

[91] C.-M. Chung, M. Qin, S. Zhang, U. Schollwöck, and S. R. White (The Simons collaboration on the many-electron problem), Plaquette versus ordinary d-wave pairing in the t'-Hubbard model on a width-4 cylinder, Phys. Rev. B **102**, 041106(R) (2020).